


Built to bite? Differences in cranial morphology and bite performance between narrow- and broad-headed European glass eels

Jens De Meyer¹  | Sam Van Wassenbergh² | Mathias Boulliart¹ |
Jelle Dhaene³ | Dominique Adriaens¹

¹Department of Biology, Evolutionary Morphology of Vertebrates, Ghent University, K.L. Ledeganckstraat 35, Ghent 9000, Belgium

²Département Adaptations du Vivant, UMR 7179 C.N.R.S./M.N.H.N., 57 rue Cuvier, Case Postale 55, Paris Cedex 05, 75231, France

³UGCT - Radiation Physics, Department of Physics and Astronomy, Ghent University, Proeftuinstraat 86, Ghent 9000, Belgium

Correspondence

Jens De Meyer, Evolutionary Morphology of Vertebrates, Ghent University, K.L. Ledeganckstraat 35, 9000 Ghent, Belgium.
Email: Jendmeyer.demeyer@ugent.be

Funding information

Special Research fund (BOF): BOF 01J05213, BOF 13/24J/052 and BOF 01D23012; Fund for Scientific Research (FWO) Grant/Award Number: 1524814N

Abstract

The presence of two phenotypes in a single species is a widespread phenomenon, also observed in European eel (*Anguilla anguilla*). This dimorphism has been related to dietary differences in the sub-adult elver and yellow eel stages, with broad-heads generally feeding on harder and/or larger-bodied prey items than narrow-heads. Nevertheless, both broad- and narrow-headed phenotypes can already be found among glass eels, the stage preceding the elver eel stage. As these glass eels are considered nonfeeding, we investigate here to what degree the observed variation in head width is reflected in variation in the musculoskeletal feeding system, as well as whether this reflects the same variation observed in the older, dimorphic yellow eels. Additionally, we investigate whether musculoskeletal differences between broad- and narrow-headed glass eels have implications on their feeding performance and could thus impact prey preference when eels start feeding. Therefore, we compared the cranial musculoskeletal system of five broad- and narrow-headed glass eels using 3D-reconstructions and simulated the glass eel's bite force using the data of the muscle reconstructions. We found that the variation in the musculoskeletal system of glass eels indeed reflects that of the yellow eels. Broader heads were related to larger jaw muscles, responsible for mouth closure. Accordingly, broad-heads could generate higher bite forces than narrow-headed glass eels. In addition, broader heads were associated with higher coronoid processes and shorter hyomandibulae, beneficial for dealing with higher mechanical loadings and consequently, harder prey. We, thus, show that head width variation in glass eels is related to musculoskeletal differences which, in turn, can affect feeding performance. As such, differences in prey preference can already take place the moment the eels start feeding, potentially leading to the dimorphism observed in the elver and yellow eel stage.

KEYWORDS

bite model, dimorphism, feeding performance, myology, osteology

1 | INTRODUCTION

Dimorphism, or the presence of two different phenotypes in a single species, is a widespread phenomenon. In most cases, dimorphism is related to differences between sexes (Lande, 1980), as examples can be found in a wide variety of species, such as fish (Aguirre & Akinpelu, 2010), frogs (Katsikaros & Shine, 1997; Maan & Cummings, 2009), lizards (Gvozdík & Van Damme, 2003), turtles (Clair, 1998), birds (Owens & Hartley, 1998; Selander, 1966), and primates (Cheverud, Dow, & Leutenegger, 1985).

Also in the yellow eel stage of the European and Japanese eel (*Anguilla anguilla* and *A. japonica*, respectively), a dimorphism can be observed: broad- and narrow-heads (Ide et al., 2011; Kaifu, Miyazaki, Aoyama, Kimura, & Tsukamoto, 2012; Kaifu, Yokouchi, Miller, Aoyama, & Tsukamoto, 2013; Lammens & Visser, 1989; Provan & Reynolds, 2000; Thurow, 1958; Törlitz, 1922). The dimorphism was validated by Ide et al. (2011), who showed that the variation in head width in yellow eels is best described by two unimodal distributions with overlapping tails, meaning specimens with an intermediate head shape are also present.

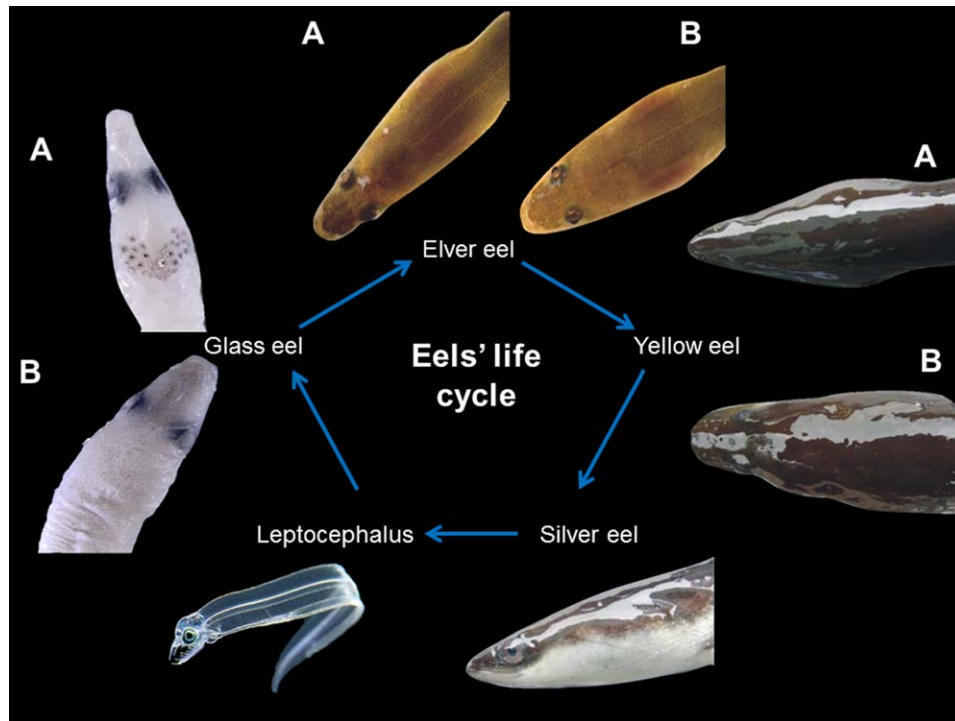


FIGURE 1 *Anguilla anguilla*, life cycle. Leptocephalus larvae hatch from the eggs in the Sargasso Sea. These larvae are transported toward the coasts of Europe, along with the Gulf stream. Arriving at the European continental shelves, they undergo metamorphosis into unpigmented glass eels, which swim up the rivers. In these rivers, eels start to feed and the eel becomes pigmented. At this stage, they are known as elver eels. Once pigmentation is complete, the eel reaches the yellow eel stage, the sedentary growth stage of the European eel. Once these eels have accumulated enough fat, they start to migrate back toward the Sargasso Sea, undergoing a final transformation to the silver eel stage. Arriving at the Sargasso Sea, these silver eels spawn and complete their life cycle. (a) Narrow-headed phenotypes. (b) Broad-headed phenotypes. © Figure leptocephalus: Fischer Aitchtuoh

The dimorphism in European eel is not sexual, but has been associated with differences in diet (De Schepper, 2007; Provan & Reynolds, 2000). Broad-headed phenotypes feed proportionally more on hard and/or large-bodied prey, such as beetles, mollusks, and fish, while narrow-heads predominantly consume soft and/or small-bodied prey, such as amphipods and chironomids (Cucherousset et al., 2011; Lammens & Visser, 1989; Provan & Reynolds, 2000; Tesch, 2003). This link between diet and head shape has recently been confirmed by a study of De Meyer, Christiaens, and Adriaens (2016), who showed that elver eels, the predecessors of the yellow eels, feeding on hard prey develop broader heads than those feeding on soft prey.

The elver eel stage (Stage VI_B of pigmentation according to Bertin, 1956) is preceded by the glass eel stage (Stage V_A-VI_A of pigmentation) (Bertin, 1956; Fukuda, Miller, Aoyama, Shinoda, & Tsukamoto, 2013) (Figure 1). These eels metamorphose from the leptocephalus larvae on arrival at the European shelf. They are nearly unpigmented and are nonfeeding during the first pigmentation stages (pigmentation Stage V_A and V_B, Bertin, 1956). The glass eels start migrating up the rivers, where they begin to feed after reaching pigmentation Stage VI_A, which can happen in a matter of days (April 2014 and April 2015). The eels then become thicker and more pigmented, turning into elver eels. Interestingly, a study on the nonfeeding glass eels showed that also in this stage, broad- and narrow-heads can be found, although the variation in head shape is not yet bimodal (De Meyer, Ide, Belpaire, Goemans, &

Adriaens, 2015), suggesting that head shape variation transitions from a unimodal to a bimodal distribution during the eel's ontogeny.

A recent gene expression analysis by De Meyer, Maes, Dirks, and Adriaens (2017) revealed that head shape variation in these glass eels could be related to differences in growth rate, since dietary differences could not have affected head shape in this stage (considering they are nonfeeding). Genes related to growth rate were upregulated in narrow-heads, suggesting that these eels grew faster than broad-headed ones. Energy not invested in growth rate could subsequently be invested in the development of the musculoskeletal system by broad-heads (De Meyer et al., 2017). As such, it is possible that the variation in head shape in glass eels is already related to variation in the musculoskeletal system. This could, in turn, allow broad-headed glass eels to start feeding on harder prey than narrow-headed glass eels once they start feeding at pigmentation Stage VI_A. Earlier research already showed that broad-headed yellow eels have larger adductor mandibulae muscles and exhibit elongated maxillaries and lower jaws with enlarged coronoids than narrow-heads (De Schepper, 2007; Goethals, 2015). These characteristics are associated with the generation of higher bite forces, allowing broad-heads to deal more efficiently with harder prey.

Using 3D-reconstructions, we want to match the observed variation in head width to variation in the musculoskeletal system in these eels and test whether this variation reflects the variation observed in the older and more developed yellow eels. Support for this would

suggest that musculoskeletal variation in the feeding system at pre-feeding could affect prey choice when the eels start feeding. This, in combination with a plastic response to the consumed prey (De Meyer et al., 2016), could then eventually lead to the dimorphism observed in the yellow eel stage. To further validate this hypothesis, we use a bite model to compare the bite forces between broad- and narrow-headed glass eels. With this study, we will, thus, be able to find out whether head shape variation in glass eels already reflects differences in feeding performance, allowing an early differentiation in diet preference between narrow- and broad-headed eelers. This will be an important step in understanding the development of the head shape dimorphism in European eel.

2 | MATERIAL AND METHODS

2.1 | Sample collection

A first sample of glass eels (*Anguilla anguilla* L.1758) was collected in the river Yser in Belgium in March 1994 ($N = 50$). A second sample was taken in April 2013 in Ostend (Belgium; $N = 200$). In both cases, a dipnet was used for sample collection. All specimens were in Stage V_A or V_B of pigment development [characterized by no external pigmentation, except for a caudal spot on the tail (V_A), the skull and some rostral pigment (V_B)] and are, therefore, considered nonfeeding (Bertin, 1956; Tesch, 2003). No prey was found in the guts accordingly. All glass eels were anesthetized with MS222 and euthanized by an MS222-overdose in accordance with Belgian legislation. The specimens were fixed in 10% formalin and preserved in 70% ethanol. Afterwards, pictures of the head were taken in dorsal view and outlines of the heads were drawn using CorelDRAW 12 (Bain & Wilkinson, 2004). These outline shapes were then used for a shape analysis as described in De Meyer et al. (2015). The shape analysis was then used to select five narrow-headed and five broad-headed specimens for further analysis, based on their distribution at the extreme ends of the PC axis describing overall head width (Figure 2a,b). To validate the outline analysis, we measured both head width (HW) just posterior to the eye and head length (HL), and calculated the HW/HL ratio. By comparing this ratio between the selected specimens, we were able to confirm that these eels were indeed narrow- and broad-heads.

2.2 | Musculoskeletal morphology

The heads of the selected specimens were removed and μ CT-scanned to study their osteology. Afterwards, the heads were treated with phosphomolybdic acid (2.5% solution for 7 days) to visualize 3D soft tissue anatomy (Metscher, 2009). The heads were then μ CT-scanned a second time, which allowed to study the cranial musculature. Heads of the 1994 and 2013 samples were scanned separately at the Centre for X-ray Tomography at Ghent University (UGCT) with the following setup: 7 kV tube voltage and 1,000 projections over 360° . The pixel pitch of the detector was $200 \mu\text{m}$ for the 1994 and 2013 samples, with the reconstructed voxel sizes being $9.88 \mu\text{m}$ and $10.269 \mu\text{m}$, respectively. The μ CT-data was then processed to generate

3D-reconstructions of the adductor mandibulae muscles in all specimens, using AMIRA 5.5.0 (Visage Imaging, San Diego, CA). Next to this, 3D-reconstructions were made of the cranial bones of seven specimens (4 broad-heads and 3 narrow-heads). Since the scan quality of the three remaining eels (1 broad-head and 2 narrow-heads) was too low to make reliable reconstructions of the complete skull, only the lower jaws of these specimens were reconstructed.

2.3 | Bite model

A static bite model is used to calculate bite forces at two positions along the lower jaw: a proximal bite point at the level of the rostral end of the eye, and a distal bite point at the tip of the lower jaw. The lower jaw is assumed to form a single rigid body that can rotate about an axis through the left and right jaw joints. Mouth-closing torque about this axis is generated by the three different adductor mandibulae bundles (A1–A3; nomenclature following Winterbottom (1973) on each side of the head. The bipennate muscle-tendon model from van Leeuwen (1992) is used to calculate the muscle forces causing this torque. The 3D-geometry of this mechanical system and the muscle model is written in Matlab Simulink version R2013b (8.2.0.701) using the SimMechanics toolbox (First Generation).

The dynamic model of a muscle-tendon complex with a bipennate muscle architecture by van Leeuwen (1992) calculates instantaneous, dynamic muscle-tendon force F_{mtc} as:

$$F_{\text{mtc}} = (F_a * F_u * F_{\text{cb0}} * \sigma_{\text{miso}} * A_{f0} * F_{\text{pas1}} + F_{\text{pas2}}) * \cos \alpha, \quad (1)$$

where F_a is a dimensionless active state factor (1 corresponds to a full, fused tetanus activation as used in the current simulations), F_u is a normalized factor to account for the force-velocity relationship (1 = isometric condition), F_{cb0} is a normalized factor for cross-bridge force under isometric conditions and full activation to account for the force-length relationship (1 = optimum fiber length), A_{f0} is the physiological cross-sectional area (muscle volume V_m divided by fiber length at rest L_{f0}), σ_{miso} the maximal isometric stress of the muscle fibers at optimal length, α the pennation angle, F_{pas1} the passive force at short fiber lengths, resisting the cross-bridge force, and F_{pas2} the passive force above optimum fiber length, acting in parallel to the cross-bridge forces.

Since tendons could not be clearly distinguished from the muscle tissue on the CT-scans, and were, thus, presumably very small, the tendon component in the model of van Leeuwen (1992) was not modeled. Bite force calculations were only done at gape angle intervals of 10° , starting with the fish in resting position with an approximately closed mouth (i.e., how they were CT-scanned) and then increasing the gape angle up to 40° . We assumed that a gape angle of 10° corresponds to the situation in which fiber lengths are optimal for active muscle force production ($F_{\text{cb0}} = 1$). Due to the absence of a tendon in the model, pennation angle will remain constant during the simulations (eqs. 7 and 8 from van Leeuwen, 1992 are not solved). Since at $F_{\text{cb0}} = 1$, F_{pas1} and F_{pas2} are typically 0, a full activation is simulated ($F_a = 1$), the pennation angle at rest (α_0) will remain constant throughout the simulation, and

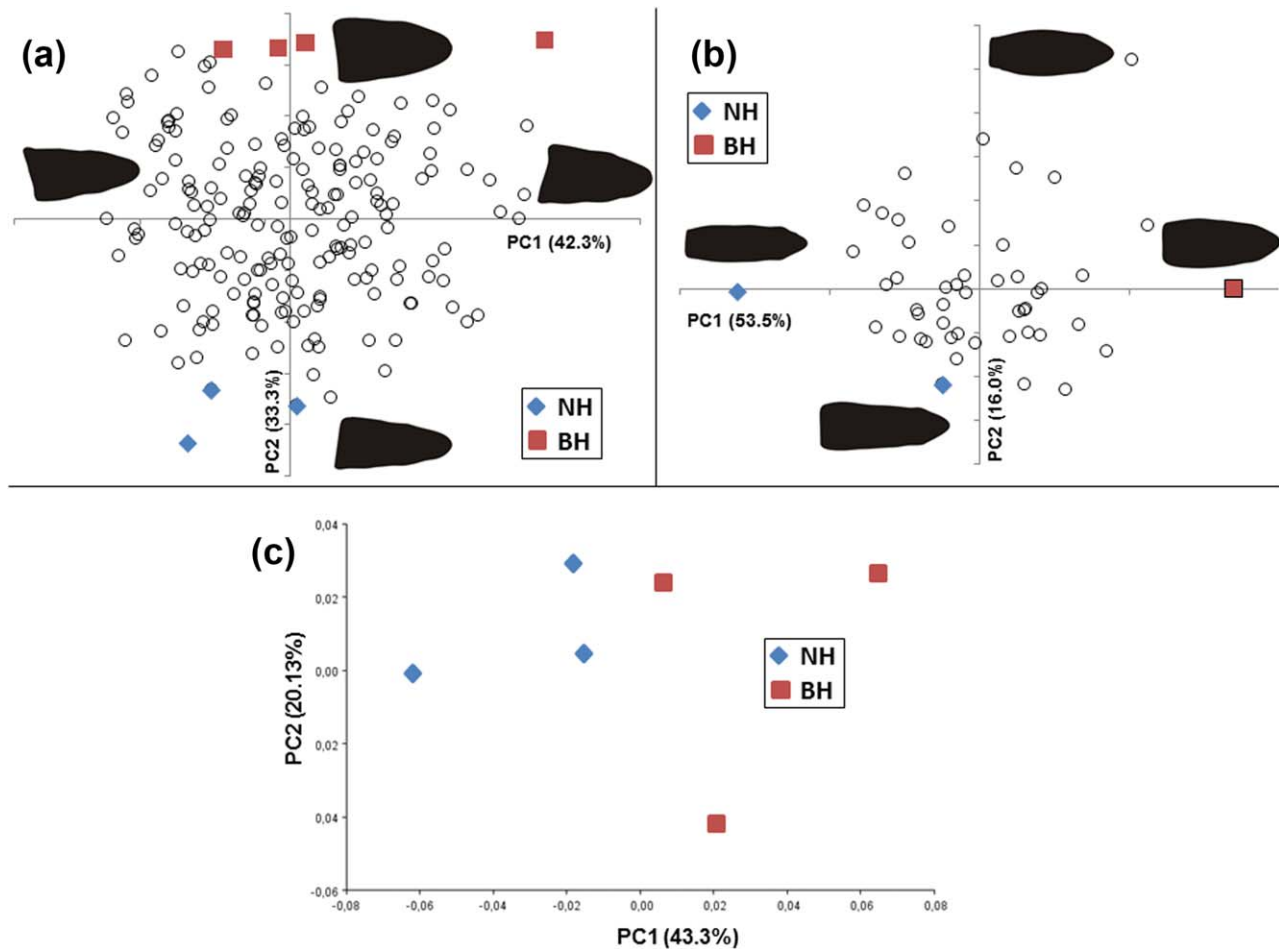


FIGURE 2 A and B: PCA on the outline shapes of the Ostend (a; $N = 200$) and Yser (b; $N = 50$) sample respectively. The colored points represent the narrow-heads (NH) and broad-heads (BH) selected for CT-scanning and further analysis. (c) PCA on the landmark-data, indicating that the shape of broad- and narrow-heads can be separated according to PC1. The head shape variation explained by the different PCs is shown in parentheses

contraction velocity is zero ($F_u = 1$), equation (Equation 1) for muscle-tendon force reduces to the following equation for muscles force F_m :

$$F_m = \sigma_{\text{miso}} * V_m / L_{f0} * \cos \alpha_0 \quad (2)$$

Maximal isometric muscle stress σ_{miso} was set to 25 N/cm^2 , as this value is commonly used for jaw muscles composed predominantly of fast, glycolytic fibers (Davis, Santana, Dumont, & Grosse, 2010; Herrel, De Smet, Aguirre, & Aerts, 2008), and also falls within the range of values measured for the adductor mandibulae of teleost fishes ($20.3 \pm 8.7 \text{ N/cm}^2$ in *Clarias gariepinus*; mean \pm SD) (Van Wassenbergh, Herrel, James, & Aerts, 2007). This value is assumed to be equal for all specimens in our sample. Volumes V_m and total muscle lengths of the three different muscles were calculated based on the 3D-reconstructions. The reported muscle volumes were calculated by averaging the muscle volumes of the left and right side of the head, as eels were assumed to be bilaterally symmetric. The pennation angle at rest α_0 of the A1 muscle bundle could not be determined based on the reconstruction. Therefore, 41.1° was used as α_0 , which is the average pennation angle in yellow eels (Goethals, 2015). Similarly, fiber length L_{f0} was estimated as $1/3$ of the total muscle length for A1 and $1/2$ of the total muscle

length for A2 and A3, as observed in yellow eels (Goethals, 2015). Finally, 3D-coordinates were collected of the insertion and origin of A1–A3, the left and right jaw joint, a proximal bite point at the rostral end of the eye, the most distal bite point and the tip of the lower jaw. The 3D-coordinates were then translated and rotated as such that all reconstructed skulls were oriented in the same direction, with the jaw joints having the coordinates (0, 0, z) and the tip of the lower jaw (x, 0, 0). Finally, these coordinates together with Equation 2 were then used to calculate the maximum bite forces of the different specimens. Since maximum bite forces were always obtained at a gape angle of 10° , only these bite forces were used for further analysis.

2.4 | Osteology

To find out whether there are differences in the osteology of narrow- and broad-headed glass eels, several measurements were taken to compare both morphotypes. Also here, when applicable, the reported measurements were calculated by averaging the measurements of the left and right side of the head. Next to this, a total of 50 3D-landmarks were used to analyze the skull shape (Figure 3). A description of the

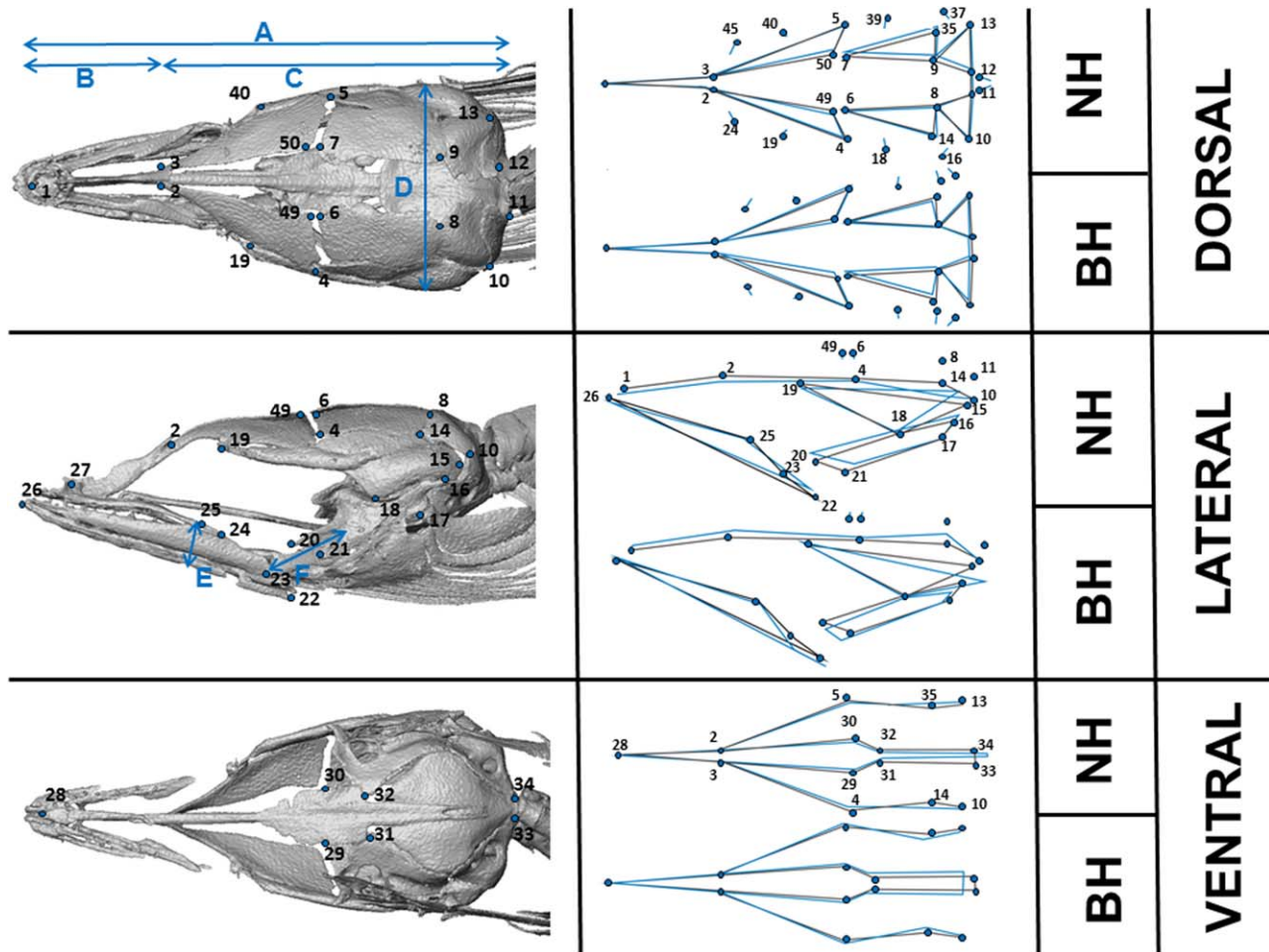


FIGURE 3 Left: the different landmarks used for the shape analysis in dorsal, lateral and ventral view. The landmark description can be found in Supporting Information Table S1. Lengths A–F correspond to the measurements A–F found in Table 1. Right: the shape of narrow-heads (NH) and broad-heads (BH) according to PC1 of the PCA on the land-mark data. Gray represents the average shape, blue the shape represented by each phenotype

landmarks and measurements can be found in Supporting Information Table S1. Landmarks were placed with Amira 5.5.0 and afterwards analyzed with MorphoJ. The variation in size, orientation, and position of the different specimens was minimized through translation, rotation, and rescaling with a Generalized Procrustes Analysis (Zelditch, Swiderski, Sheets, & Fink, 2004). Afterwards, a principal component analysis (PCA) was performed on the landmark data to detect the major axes of shape variation of the skull.

2.5 | Statistics

A nonparametric permutation test (10,000 replicates) in PAST (Hammer, Harper, & Ryan, 2001) was used to find significant differences in HW/HL, relative skull measurements, absolute and relative muscle length (corrected for total length) and scaled muscle volume between broad- and narrow-heads. The scaled muscle volume was calculated as the cube root of the muscle volumes divided by total body length. In addition, an ANCOVA with total body length as covariate was performed to find significant differences in bite force and absolute muscle volume between narrow- and broad-headed glass eels. Finally,

we tested whether HW/HL was correlated with the absolute and scaled muscle volumes and bite forces using a Pearson correlation test.

3 | RESULTS

3.1 | Shape analysis

PC1 of the shape analysis on the Ostend sample explained 42.3% of the total variation. Most of the head shape variation was mainly related to differences at the posterior end of the head and partially to differences in head width (Figure 2a). As PC2 (33.3%) reflected almost exclusively variation in head width, it was chosen to select broad- and narrow-heads for further analysis. Because of the larger sample size of the Ostend sample, more specimens were selected than from the Yser sample (4 broad-heads (BH) and 3 narrow-heads (NH) based on the shape analysis). For the Yser sample, both PC1 (53.5%) and PC2 (16.0%) were related to variation in head width. According to PC1, both the most narrow- and broad-headed specimen was selected. In addition, the most narrow-headed specimen according to PC2 was chosen (Figure 2b). The permutation test confirmed these observations

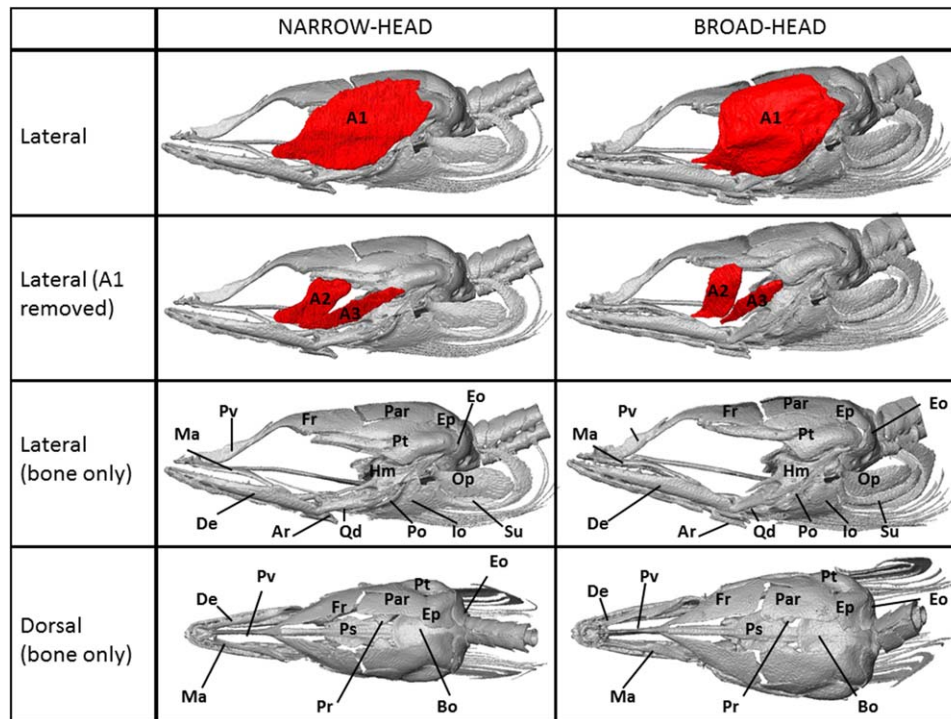


FIGURE 4 The muscle and bone configuration of a narrow- and broad-headed glass eel. A1–3: Adductor mandibulae 1–3. Ar: Articulare. Bo: Basioccipital. De: Dentary. Eo: Exoccipital. Ep: Epiotic. Fr: Frontal. Hm: Hyomandibula. Io: Interopercular. Ma: Maxilla. Op: Opercular. Par: Parietal. Po: Preopercular. Pr: Prootic. Ps: Parasphenoid. Pt: Pterotic. Pv: Premaxillo-vomercomplex. Qd: Quadrate. Su: subopercular

as broad- and narrow-heads differed significantly in HW/HL (BH: $0.49 \pm .03$; NH: $0.38 \pm .05$; p value: .007).

3.2 | Osteology

The skull of narrow- and broad-heads is highly comparable and the description below is, therefore, applicable for both phenotypes. The neurocranium is not yet completely ossified. The left and right frontals, parietals, epiotics, and exoccipitals are not fused, leaving a large, dorso-medial fontanel in between (Figure 4). No complete fusion has taken place between these bones and the dorsal edge of the pterotic as well, leaving several smaller fontanel (Figure 4). Other fontanel can still be observed between the parietal and frontal, between the parasphenoid and the prootic and between the basioccipital and the prootic. Interestingly, the sphenotic is still completely absent in the glass eel stage (Figure 4), while the basisphenoid and pterosphenoid are still cartilaginous. None of the measurements differed significantly between narrow- and broadheads when corrected for body size (Table 1), which can be a consequence of the low sample size. Nevertheless, considering that glass eels are still small and not actively feeding, we observe that both the upper and lower jaw were slightly longer in broad-heads. Next to this, they exhibit a higher coronoid process, a shorter hyomandibula and a broader, but shorter skull, features that are also typical for broad-headed yellow eels (Table 1).

For the landmark analysis, six specimens were used (three narrow- and three broad-heads), since not all landmarks could be reliably determined in one of the broad-heads. PC1, explaining 43.3% of the total variation, represents the narrow- to broad-head axis (Figure 2c). The

differences in shape confirm the observations of the measurements. Both in dorsal and ventral view, we observe that broad-heads have a shortened but broader skull. Interestingly, the dorso-medial fontanel is narrower in broad-heads, as the distances between the left and right frontals, parietals, epiotics, and exoccipitals are shortened. In lateral view, a shortened lower and upper jaw is observed in the narrow-heads. Next to this, the skull of the broad-heads seems to be higher in broad-heads, which is characteristic for broad-headed yellow eels. PC2 (20.13%), PC3 (15.23%), and PC4 (11.93%) did not show differences between the two phenotypes and were, therefore, not used for further analysis.

3.3 | Myology

Origin and insertion of the different muscles were similar for both morphotypes (Figure 4). The adductor mandibulae can be subdivided in three parts (A1–A3). The origin of the large A1 muscle bundle extends over the dorso-lateral surface of the frontal, parietal and pterotic while inserting on the caudal edge of the coronoid process. The A1 bundles, however, do not yet cover the complete skull, as they do in yellow eels. Medial to A1, A2 stretches from the cartilaginous basisphenoid and pterosphenoid to the caudal margin of the coronoid and the medial surface of the dentary. A3, finally, is a long muscle bundle that originates from lateral surface of the hyomandibula and inserts on the medial dentary surface. The lengths of the different muscle bundles were highly comparable for both phenotypes, even when corrected for total body size, and, therefore, no significant differences are found (Table 2). While the length of the muscles did not differ between the

TABLE 1 Average \pm SD of both the absolute as relative lengths measured in narrow-heads (NH; $N = 3$) and broad-heads (BH; $N = 4$)

		Absolute (mm)			Size correction		
		NH	BH	p	NH	BH	p
A	Length complete skull	4.87 \pm 0.15	4.67 \pm 0.23	0.25	.076 \pm .003	.073 \pm .001	.1
B	Premaxillo-Ethmoidvomer complex	1.71 \pm 0.13	1.68 \pm .01	0.83	.027 \pm .001	.026 \pm .001	.66
C	Length neurocranium	3.31 \pm .06	3.29 \pm 0.21	0.89	.052 \pm .003	.051 \pm .003	.75
D	SW bulbs pterotic	1.83 \pm .02	1.92 \pm 0.13	0.29	.029 \pm .002	.030 \pm .002	.43
E	Height Coronoid	0.44 \pm .03	0.46 \pm .01	0.15	.0068 \pm .0006	.0072 \pm .0003	.19
F	Length Quadrate	1.02 \pm 0.11	1.01 \pm .08	0.78	.016 \pm .002	.016 \pm .002	.97
G	Length frontal (LM 2-49; 3-50)	1.59 \pm .01	1.61 \pm .14	0.84	.025 \pm .002	.025 \pm .002	.96
H	length parietal (LM 6-8; 7-9)	1.15 \pm .01	1.13 \pm .09	0.88	.018 \pm .001	.018 \pm .001	.53
I	SW rostral tips pterotic (LM 19-40)	1.21 \pm .03	1.28 \pm .02	.01	.019 \pm .002	.020 \pm .001	.34
J	SW distal ends frontal (Lm 4-5)	1.42 \pm .01	1.54 \pm .09	0.11	.022 \pm .001	.024 \pm .001	.09
K	SW lateral ends epioccipitals (LM 10-13)	1.41 \pm .01	1.41 \pm .05	0.97	.022 \pm .002	.022 \pm .001	.87
L	Length hyomandibular (LM 16-21)	1.97 \pm .01	1.86 \pm .03	.01	.031 \pm .002	.029 \pm .001	.14
M	Length Lower Jaw (LM 22-26; 43-47)	2.86 \pm 0.10	2.93 \pm 0.20	0.51	.044 \pm .003	.046 \pm .001	.25
N	Length upper jaw (LM 24-26; 45-48)	1.48 \pm .09	1.51 \pm 0.15	0.73	.023 \pm .002	.024 \pm .002	.81
O	Length Pteroric (LM 15-19; 36-40)	2.25 \pm 0.12	2.23 \pm .08	0.77	.035 \pm .001	.035 \pm .001	.49

* indicate significant differences ($p < .05$). Lengths A--F correspond to the measurements shown in Figure 3. Lengths G--O are measured between the mentioned landmarks and are averaged for the left and right side where applicable.

two phenotypes, the volumes did show strong differences. All scaled muscle volumes were significantly larger in broad-heads compared to narrow-heads (Table 2). Figure 5 confirms these observations,

indicating that, when comparing specimens of similar length, broad-heads tend to have larger muscle volumes. Accordingly, the correlation test showed that HW/HL was positively correlated with both the

TABLE 2 Average \pm SD of the bite force (BF), total length (TL), and both absolute and scaled volume of the different adductor mandibulae muscle bundles and the sum of these muscle bundles measured in narrow-heads (NH; $N = 5$) and broad-heads (BH; $N = 5$)

	A1				A2			
	NH	BH	p	Sl. Eq.	NH	BH	p	Sl. Eq.
Proximal BF (mN)	11.88 \pm 4.51	19.1 \pm 3.06	.001	0.54	2.71 \pm 1.12	4.92 \pm 1.54	.002	0.20
Distal BF (mN)	6.19 \pm 2.66	10.09 \pm 1.98	.01	0.31	1.45 \pm 0.50	2.57 \pm 0.76	.002	0.27
TL (mm)	2.56 \pm 0.19	2.69 \pm .05	0.24	-	1.18 \pm 0.18	1.21 \pm 0.11	0.76	-
Relative TL	.040 \pm .002	.042 \pm .002	0.12	-	.018 \pm .002	.019 \pm .002	0.64	-
Volume (mm ³)	0.191 \pm .073	0.303 \pm .065	.01	0.42	.021 \pm .005	.028 \pm .006	.03	0.48
Volume scaled	.0088 \pm .0009	.0104 \pm .0008	.02	-	.0043 \pm .0003	.0047 \pm .0002	.02	-
	A3				Σ A1-A3			
	NH	BH	p	Sl. Eq.	NH	BH	p	Sl. Eq.
Proximal BF (mN)	1.03 \pm 0.61	1.76 \pm 0.40	.03	0.13	15.41 \pm 6.06	25.74 \pm 4.47	.001	0.71
Distal BF (mN)	0.40 \pm 0.26	0.88 \pm 0.23	.08	0.16	9.05 \pm 3.46	13.54 \pm 2.70	.002	0.42
TL (mm)	1.28 \pm 0.44	1.37 \pm 0.21	0.68	-	-	-	-	-
Relative TL	.020 \pm .006	.021 \pm .002	0.54	-	-	-	-	-
Volume (mm ³)	.014 \pm .006	.020 \pm .004	.03	0.29	0.243 \pm .081	0.350 \pm .072	.01	0.44
Volume scaled	.0036 \pm .0004	.0042 \pm .0003	.02	-	.0093 \pm .0010	.0110 \pm .0007	.01	-

Also, the p value for slope equality (Sl. Eq.) is given, which should be higher than .05 to perform an ANCOVA.

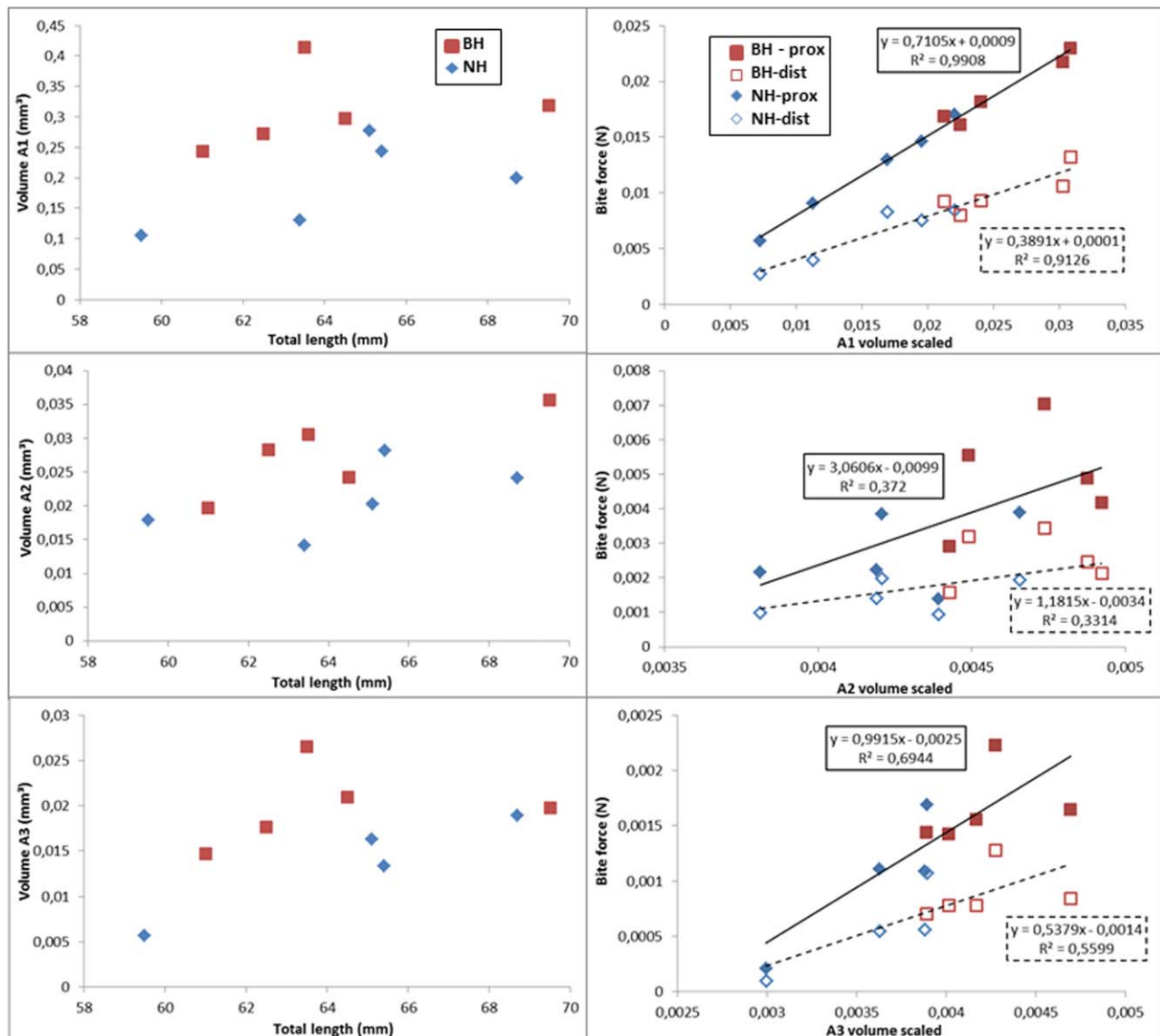


FIGURE 5 Left: Relation between the volumes of the different adductor mandibulae muscle bundles and the length of the specimens, indicating that especially A1 and A3 are larger in broad-heads when comparing specimens of similar length. Right: Relation between the bite force generated by each adductor mandibulae muscle bundle and their scaled volume, indicating that larger volumes can generate higher bite forces. The linear regression is not significant between the scaled A2 volume and bite force ($p = .06$), while the regressions for the scaled A1 and A3 volumes were significant ($p < .05$). Full line: linear regression of proximal bite force on muscle volume. Dashed line: linear regression of distal bite force on muscle volume

absolute and scaled muscle volumes. Still, these were only significant for the absolute volume of A1 and the scaled volumes of A1 and A2 (Table 3). Nevertheless, all these analyses strongly suggest that variation in head width can already be linked to variation in muscle volume in the glass eel stage, with broader heads being associated with larger jaw muscles.

3.4 | Bite force

The data from the adductor mandibulae reconstructions were used to calculate the bite force of the glass eels. Most of the bite force is generated by A1, being approximately 4 times larger than by A2 and 13.5 times larger than by A3 (Figure 6). The proximal bite force was about

twice as high as the distal one in both broad- and narrow-heads (Table 2). Bite forces showed a strong increase with scaled muscle volume, especially A1 (Figure 5) indicating that larger volumes can generate higher bite forces, assuming that no changes in muscle architecture take place. As such, it can be expected that the larger adductor mandibulae volumes of broad-heads, thus, allow them to exhibit higher bite forces. Indeed, we observed that all three muscle bundles generated a bite force that was larger in broad-heads compared to narrow-heads, although the differences were only significant for A1 and A2 (Table 2). The total bite force, estimated as the sum of the bite forces of A1, A2, and A3, was significantly larger in the broad-headed specimens both at the proximal and distal bite point (Table 2). This strongly suggests that broad-heads can generate a larger bite force than narrow-heads, even

TABLE 3 Results of the correlation analysis between the absolute and scaled muscle volumes and bite force with the head width/head length ratio, showing both the correlation value (R) and the p values of the correlation value

		R	p
Absolute volume (mm ³)	A1	0.78	.01
	A2	0.61	.06
	A3	0.51	0.16
Scaled volume	A1	0.78	.01
	A2	0.67	.03
	A3	0.56	0.12
Bite force (N)	proximal	0.67	.03
	distal	0.64	.04

for eels that have the same size (Figure 6). Indeed, a significant, positive correlation was found between HW/HL and the proximal and distal bite force (Table 3), indicating that glass eels with broader heads should be capable to generate higher bite forces.

4 | DISCUSSION

In this study, we want to determine the musculoskeletal variation underlying the observed variation in head width in glass eels. The glass eels in our study are in pigmentation Stage V_A or V_B and are, therefore,

considered nonfeeding. However, these eels start feeding after reaching pigmentation Stage VI_A, which can happen in a matter of days (April 2014 and April 2015;). As such, musculoskeletal differences related to head width differences in glass eels could already result in variation in feeding performance, which can become apparent when feeding starts. Using 3D-reconstructions, we found that broader heads in glass eels were associated with larger jaw muscles. An earlier study on air-breathing catfishes indicated that species with larger jaw adductors are capable of generating higher bite forces (Herrel, Adriaens, Verraes, & Aerts, 2002). Similarly, a study on finches showed that fringillids can generate higher bite forces than estrilids of similar size because they have relatively larger jaw muscles (van der Meij & Bout, 2004). Also in lizards, broader heads associated with larger jaw muscles are related to higher bite forces. (Herrel, McBrayer, & Larson, 2007; Verwajen, Van Damme, & Herrel, 2002). Finally, even in humans, masseter muscle thickness shows a significant positive correlation with bite force (Raadsheer, Van Eijden, van Ginkel, & Prah-Andersen, 1999). As such, larger jaw muscles allow the generation of higher bite forces. This pattern is confirmed by the bite force simulations in our study as the larger jaw muscles of broad-headed glass eels are related to higher bite forces.

Also variation in the skeletal system has the potential to influence bite force. Our analysis shows that glass eels with broader heads have relatively longer upper and lower jaws and a heightened coronoid process, which acts as insertion site for the jaw muscles. As such, a higher coronoid process provides a larger attachment surface for the

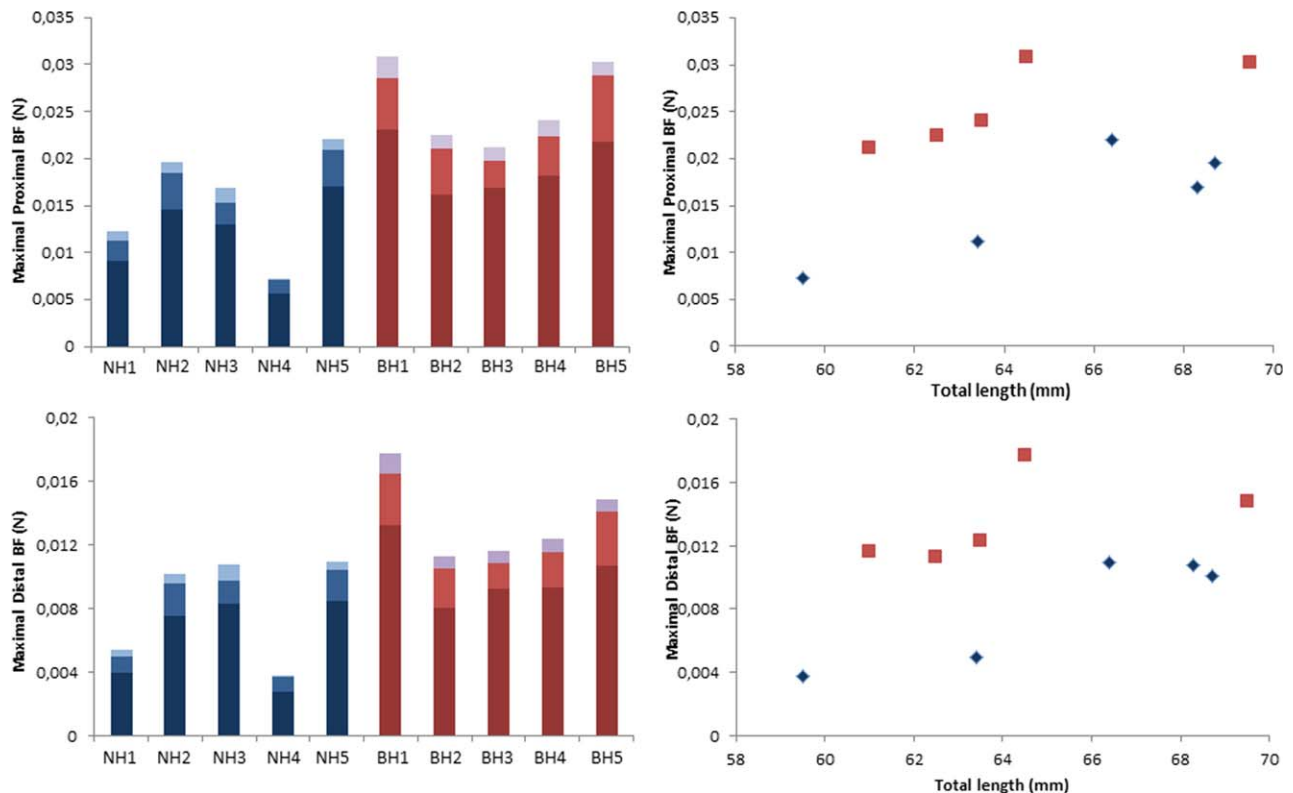


FIGURE 6 Left: Proximal and distal bite force generated by the different adductor mandibulae muscle bundles in each specimen. Right: Relation between the total bite force (estimated as the sum of the bite forces generated by each adductor mandibulae muscle bundle) and total length, indicating that broad-heads can exhibit larger bite forces than narrow-heads of similar length

jaw muscles and a longer force input arm. Both these factors show a positive relation with bite force (Cabuy, Adriaens, Verraes, & Teugels, 1999; Herrel et al., 2002). Interestingly, longer lower jaws are known to decrease bite force as they increase the outlever of the jaw system (Herrel, De Grauw, & Lemos-Espinal, 2001; Verwajen et al., 2002). However, European eels are known to perform three types of feeding behavior: suction, biting, and spinning behavior (Helfman & Winkelman, 1991). Spinning behavior is generally applied for large, hard prey items and will thus mainly be used by broad-headed phenotypes. During spin feeding, the eel grabs a prey item in the mouth and spins along its long axis to tear of smaller pieces. Longer lower jaws and the associated longer tooth batteries of broad-heads might thus improve their grip on large prey items during spinning behavior. Eels also generally only use the posterior end and not the tip of the mouth to bite on prey items and the longer lower jaw might, thus, have little influence on bite force (April - September 2015;). In addition, it is possible that the longer force input arm, associated with the taller coronoid, compensates a possible loss in bite force due to a longer outlever in broad-heads. The bite force model indeed shows that even at a distal bite point, broad-heads can generate a higher bite force than narrow-heads. Finally, we observed that broad-headed glass eels exhibit a relatively broader skull, which might allow the accommodation of larger muscles and could provide more support to deal with higher mechanical loads associated with higher bite forces.

Based on the aforementioned observations, we can conclude that head width variation in glass eels is associated with musculoskeletal variation in the feeding system that can be linked to bite force and feeding performance. Differences in bite force, in turn, are associated with diet diversity (Clifton & Motta, 1998; Wainwright, 1988) and resource partitioning (Verwajen et al., 2002; Wiersma, 2001). Males of the lizard *Podarcis hispanica atrata* (Steindacher, 1870), for example, have broader heads, allowing the generation of higher bite forces and the consumption of larger prey items than females (Herrel, Van Damme, & De Vree, 1996). Similarly, female filesnakes (*Acrochordus arafurae* McDowell, 1979) have larger heads than males and can consequently take up prey items up to 500 g, whereas males can only consume prey items up to 100 g (Shine, 1986). Several species of Caribbean wrasses (Labridae) are able to co-occur in coral reefs, as species with high crushing forces eat harder-shelled prey than species with lower crushing forces (Wainwright, 1988). Differences in head width in the yellow eel stage of the European eel have also been related to resource partitioning (De Schepper, 2007; Goethals, 2015), with broad-heads consuming hard and large prey, such as crustaceans and fish and narrow-heads mainly consuming soft and small benthic invertebrates (Lammens & Visser, 1989; Provan & Reynolds, 2000; Tesch, 2003). Interestingly, the musculoskeletal variation underlying head width variation is highly similar between the young, nonfeeding glass eels and the older, feeding yellow eels (De Schepper, 2007; Goethals, 2015). In a recent study, De Meyer et al. (2017) suggested that the prefeeding variation in head width could be caused by differences in growth rate, with fast-growing glass eels developing narrower heads than slow-growing glass eels. In this study, we show that this variation in head shape at prefeeding, even when induced by differences in growth rate,

can also be related to variation in the musculoskeletal feeding system and feeding performance. Broad-headed glass eels exhibit a musculoskeletal design that makes them better suited to start feeding on harder, larger-bodied prey items than narrow-headed ones. Indeed, higher bite forces can be important during both shaking and spinning behavior, as a powerful grasp on the prey item is necessary to rip tissue and to avoid damage to the teeth and jaws (Gerry, Summers, Wilga, & Dean, 2010). Furthermore, the differences in bite force might allow the broad-headed eels to access mechanically challenging prey items earlier in life than narrow-headed ones (Kolmann & Huber, 2009). The initial differences in feeding performance might, thus, be a way to lower intra-specific competition among young eels that start feeding (Schoener, 1974). Indeed, in a study of De Meyer et al. (2016), it was shown that when eels are given both hard and soft prey items, some eels will develop a broad head and others a narrow head, suggesting that some eels actively prefer hard over soft prey and vice versa. As such, the initial head shape variation, although not yet bimodal in glass eels (De Meyer et al., 2015), could eventually lead to the bimodal distribution observed in yellow eels, as it is already associated with variation in musculoskeletal design and bite force.

However, we need to note that we do not know whether the calculated bite forces match with the actual bite forces, since no in vivo bite forces have been measured on glass eels. The calculated bite forces should be critically evaluated because of several factors. First of all, the pennation angle of the A1 muscle bundle nor tendon length could be determined from the reconstructions. Next to this, the fiber length of the different muscles could not be measured, since the CT-data did not allow to identify individual fibers. These factors represent important components of the muscle architecture. As broad-heads could start feeding on larger prey items than narrow-heads, this could have an impact on their muscle architecture and the two phenotypes might consequently differ in these components, possibly affecting the calculated bite forces. Previous research, however, showed that both fiber lengths and pennation angles were similar between broad- and narrow-headed yellow eels (Goethals, 2015), suggesting that the higher bite forces of broad-heads are mainly related to an increased muscle volume, rather than to differences in pennation angle and fiber length. Furthermore, an earlier sensitivity analysis showed that changing the pennation angle with 5° only results in a bite force change of approximately 7% (March 2016). As such, the differences in calculated bite force between the two phenotypes can be considered as a reliable estimation of the actual difference. Still, differences in the size of the consumed prey items between broad- and narrow-heads might also lead to differences in muscle physiology parameters, such as for example variation in the force-length relationship, which could not be evaluated in this study.

In conclusion, this study shows that the musculoskeletal variation underlying the head width variation in nonfeeding glass eels is identical to the variation observed in the yellow eel stage. Broader heads were associated with larger jaw muscles, longer upper and lower jaws and a heightened coronoid. Such a design is associated with higher bite forces and facilitates the consumption of harder prey items. Therefore, it is possible that broader-headed eels consume more hard prey items

than narrow-headed ones when feeding starts, which could eventually lead to the dimorphism observed in yellow eels.

ACKNOWLEDGMENTS

The authors would like to thank the personnel of ANB (Agency for Nature and Forest) for providing the Yser sample collection. The authors are also indebted to the personnel of INBO (Institute for Nature and Forest Research) for their help with the Ostend sample collection. The project was funded by the Special Research fund (project code: BOF 01J05213). Also J. De Meyer and M. Bouilliant were funded by the Special Research Fund (BOF) of Ghent University (BOF 13/24J/052 and BOF 01D23012 respectively). S. Van Wassenbergh was funded by the Fund for Scientific Research (FWO: grant 1524814N).

AUTHOR CONTRIBUTIONS

De Meyer J. was responsible for the head shape analyses, the 3D-reconstructions of the glass eels, analysis of the musculoskeletal morphology and calculation of the bite forces. Bouilliant M. assisted with the bite model and the 3D-reconstructions. Dhaene J. was responsible for the μ CT-scanning. Finally, Adriaens D. acted as supervisor of the experiment, advised about the applied methods and helped writing the manuscript.

ORCID

Jens De Meyer  <http://orcid.org/0000-0003-2884-0469>

REFERENCES

- Aguirre, W. E., & Akinpelu, O. (2010). Sexual dimorphism of head morphology in three-spined stickleback *Gasterosteus aculeatus*. *Journal of Fish Biology*, 77(4), 802–821.
- Bain, S., & Wilkinson, N. (2004). *CorelDRAW 12: The official guide* (695 p.). New York, United States: Mc Graw Hill Professional.
- Bertin, L. (1956). *Eels: A biological study* (192. p.). London, UK: Cleaver-Hume Press.
- Cabuy, E., Adriaens, D., Verraes, W., & Teugels, G. G. (1999). Comparative study on the cranial morphology of *Gymnallabes typus* (Siluriformes: Clariidae) and their less anguilliform relatives, *Clariallabes melas* and *Clarias gariepinus*. *Journal of Morphology*, 240, 169–194.
- Cheverud, J. M., Dow, M. M., & Leutenegger, W. (1985). The quantitative assessment of phylogenetic constraints in comparative analyses: Sexual dimorphism in body weight among primates. *Evolution*, 39, 1335–1351.
- Clair, R. C. S. (1998). Patterns of growth and sexual size dimorphism in two species of box turtles with environmental sex determination. *Oecologia*, 115, 501–507.
- Clifton, K. B., & Motta, P. J. (1998). Feeding morphology, diet and ecomorphological relationships among five Caribbean labrids (Teleostei, Labridae). *Copeia*, 1998, 953–966.
- Cucherousset, J., Acou, A., Blanchet, S., Britton, J. R., Beaumont, W. R. C., & Gozlan, R. E. (2011). Fitness consequences of individual specialisation in resource use and trophic morphology in European eels. *Oecologia*, 167(1), 75–84.
- Davis, J. L., Santana, S. E., Dumont, E. R., & Grosse, I. R. (2010). Predicting bite force in mammals: Two-dimensional versus three-dimensional lever models. *Journal of Experimental Biology*, 213(11), 1844–1851.
- De Meyer, J., Christiaens, J., & Adriaens, D. (2016). Diet-induced phenotypic plasticity in European eel (*Anguilla anguilla*). *Journal of Experimental Biology*, 219, 354–363.
- De Meyer, J., Ide, C., Belpaire, C., Goemans, G., & Adriaens, D. (2015). Head shape dimorphism in European glass eels (*Anguilla anguilla*). *Zoology*, 118(6), 413–423.
- De Meyer, J., Maes, G. E., Dirks, R. P., & Adriaens, D. (2017). Differential gene expression in narrow- and broad-headed European glass eels (*Anguilla anguilla*) points to a transcriptomic link of head shape dimorphism with growth rate and chemotaxis. *Molecular Ecology*, 26(15), 3943–3953.
- De Schepper, N. (2007). *Evolutionary morphology of body elongation in teleosts: Aspects of convergent evolution* (PhD dissertation, 292 p.). Ghent, Belgium: Ghent University.
- Fukuda, N., Miller, M. J., Aoyama, J., Shinoda, A., & Tsukamoto, K. (2013). Evaluation of the pigmentation stages and body proportions from the glass eel to yellow eel in *Anguilla japonica*. *Fisheries Science*, 79(3), 425–438.
- Gerry, S. P., Summers, A. P., Wilga, C. D., & Dean, M. N. (2010). Pairwise modulation of jaw muscle activity in two species of elasmobranchs. *Journal of Zoology*, 281, 282–292.
- Goethals, T. (2015). *Head shape dimorphism en European eels (Anguilla anguilla): Assessing myology and bite force in broadheads and narrow-heads* (Master's thesis, 29 p.). Ghent, Belgium: Ghent University.
- Gvozdk, L., & Van Damme, R. (2003). Evolutionary maintenance of sexual dimorphism in head size in the lizard *Zootica vivipara*: A test of two hypotheses. *Zoological Society of London*, 259, 7–13.
- Hammer, O., Harper, D. A. T., & Ryan, P. D. (2001). Past: Paleontological statistics software package for education and data analysis. *Palaeo Electronica*, 4, 1–9.
- Helfman, G. S., & Winkelman, D. L. (1991). Energy trade-offs and foraging mode choice in American eels. *Ecology*, 72(1), 310–318.
- Herrel, A., Adriaens, D., Verraes, W., & Aerts, P. (2002). Bite performance in clariid fishes with hypertrophied jaw adductors as deduced by bite modeling. *Journal of Morphology*, 253(2), 196–205.
- Herrel, A., De Grauw, E., & Lemos-Espinal, J. A. (2001). Head shape and bite performance in *Xenosaurid* lizards. *Journal of Experimental Zoology*, 290, 101–107.
- Herrel, A., De Smet, A., Aguirre, L. F., & Aerts, P. (2008). Morphological and mechanical determinants of bite force in bats: Do muscles matter? *Journal of Experimental Biology*, 211(1), 86–91.
- Herrel, A., McBrayer, L. D., & Larson, P. M. (2007). Functional basis for sexual differences in bite force in the lizard *Anolis carolinensis*. *Biological Journal of the Linnean Society*, 91, 111–119.
- Herrel, A., Van Damme, R., & De Vree, F. (1996). Sexual dimorphism of head size in *Podarcis hispanica atrata*: Testing the dietary divergence hypothesis by bite force analysis. *Netherlands Journal of Zoology*, 46, 253–262.
- Ide, C., De Schepper, N., Christiaens, J., Van Liefferinge, C., Herrel, A., Goemans, G., ... Adriaens, D. (2011). Bimodality in head shape in European eel. *Journal of Zoology*, 285(3), 230–238.
- Kaifu, K., Miyazaki, S., Aoyama, J., Kimura, S., & Tsukamoto, K. (2012). Diet of Japanese eels *Anguilla japonica* in the Kojima Bay-Asahi River system, Japan. *Environmental Biology of Fishes*, 96(4), 439–446.
- Kaifu, K., Yokouchi, K., Miller, M. J., Aoyama, J., & Tsukamoto, K. (2013). Head-shape polymorphism in Japanese eels *Anguilla japonica* in relation to differences of somatic growth in freshwater and brackish habitats. *Journal of Fish Biology*, 82(4), 1308–1320.
- Katsikaros, K., & Shine, R. (1997). Sexual dimorphism in the tusked frog, *Adelotus brevis* (Anura: Myobatrachidae): The roles of natural and sexual selection. *Biological Journal of the Linnean Society*, 60, 39–51.

- Kolmann, M. A., & Huber, D. R. (2009). Scaling of feeding biomechanics in the horn shark *Heterodontus francisci*: Ontogenetic constraints on durophagy. *Zoology*, 112(5), 351–361.
- Lammens, E. H. R. R., & Visser, J. T. (1989). Variability of mouth width in European eel, *Anguilla anguilla*, in relation to varying feeding conditions in three Dutch lakes. *Environmental Biology of Fishes*, 26, 63–75.
- Lande, R. (1980). Sexual dimorphism, Sexual selection and adaptation in polygenic characters. *Evolution*, 34, 292–305.
- Maan, M. E., & Cummings, M. E. (2009). Sexual dimorphism and directional sexual selection on aposematic signals in a poison frog. *Proceedings of the National Academy of Sciences of the United States of America*, 106(45), 19072–19077.
- McDowell, S. B., (1979). A catalogue of the snakes of New Guinea and the Solomons, with special reference to those in the Bernice P. Bishop Museum. Part 3. Boinae and Acrochordoidea (Reptilia, Serpentes). *Journal of Herpetology*, 13(1), 105–111.
- Metscher, B. D. (2009). MicroCT for developmental biology: A versatile tool for high-contrast 3D imaging at histological resolutions. *Developmental Dynamics*, 238(3), 632–640.
- Owens, I. P. F., & Hartley, I. R. (1998). Sexual dimorphism in birds: Why are there so many different forms of dimorphism. *Proceedings of the Royal Society B*, 265, 397–407.
- Proman, J. M., & Reynolds, J. D. (2000). Differences in head shape of the european eel. *Fisheries Management and Ecology*, 7, 349–354.
- Raadsheer, M. C., Van Eijden, T. M., van Ginkel, F. C., & Prah-Andersen, B. (1999). Contribution of Jaw muscle and craniofacial morphology to human bite force magnitude. *Journal of Dental Research*, 78(1), 31–42.
- Schoener, T. W. (1974). Resource partitioning in ecological communities. *Science*, 185, 27–39.
- Selander, R. K. (1966). Sexual dimorphism and differential niche utilization in birds. *The Condor*, 68, 113–151.
- Shine, R. (1986). Sexual differences in morphology and niche utilization in an aquatic snake, *Acrochordus afafuræ*. *Oecologia*, 69, 260–267.
- Tesch, F. W. (2003). *The eel*. Oxford: Blackwell Science.
- Thurrow, F. (1958). Untersuchungen über die spitz und breitköpfigen Varianten des Flusssaales. *Archiv Für Fischereiwissenschaft*, 9, 79–97.
- Törlitz, H. (1922). Anatomische und entwicklungsgeschichtliche Beiträge zur Artfrage unseres Flusssaales. *Zeitschrift Für Fisch*, 21, 1–48.
- van der Meij, M. A. A., & Bout, R. G. (2004). Scaling of jaw muscle size and maximal bite force in finches. *Journal of Experimental Biology*, 207(16), 2745–2753.
- van Leeuwen, J. L. (1992). Muscle function in locomotion. In R. M. Alexander (Ed.), *Mechanics of animal locomotion* (pp. 191–250). Heidelberg: Springer-Verlag.
- Van Wassenbergh, S., Herrel, A., James, R. S., & Aerts, P. (2007). Scaling of contractile properties of catfish feeding muscles. *Journal of Experimental Biology*, 210(7), 1183–1193.
- Verwajen, D., Van Damme, R., & Herrel, A. (2002). Relationships between head size, bite force, prey handling efficiency and diet in two sympatric lacertid lizards. *Functional Ecology*, 16, 842–850.
- Wainwright, P. C. (1988). Morphology and ecology: Functional basis of feeding constraints in Caribbean labrid fishes. *Ecology*, 69, 635–645.
- Wiersma, J. H. (2001). *Maximum estimated bite force, skull morphology, and primary prey size in North American carnivores* (179. p.). Ontario, Canada: Laurentian University.
- Winterbottom, R. (1973). A descriptive synonymy of the striated muscles of the Teleostei. *Proceedings of the Academy of Natural Sciences of Philadelphia*, 125, 225–317.
- Zelditch, M. L., Swiderski, D. L., Sheets, H. D., & Fink, W. L. (2004). *Geometric morphometrics for biologists: A primer* (437. p.). New York and London: Elsevier Academic Press.

SUPPORTING INFORMATION

Additional Supporting Information may be found online in the supporting information tab for this article.

How to cite this article: De Meyer J, Van Wassenbergh S, Bouilliart M, Dhaene J, Adriaens D. Built to bite? Differences in cranial morphology and bite performance between narrow- and broad-headed European glass eels. *Journal of Morphology*. 2018;279:349–360. <https://doi.org/10.1002/jmor.20776>